Journal of
Materials Chemistry A

Accepted Manuscript

This is an *Accepted Manuscript*, which has been through the RSC Publishing peer review process and has been accepted for publication.

Accepted Manuscripts are published online shortly after acceptance, which is prior to technical editing, formatting and proof reading. This free service from RSC Publishing allows authors to make their results available to the community, in citable form, before publication of the edited article. This *Accepted Manuscript* will be replaced by the edited and formatted *Advance Article* as soon as this is available.

To cite this manuscript please use its permanent Digital Object Identifier (DOI®), which is identical for all formats of publication.

More information about *Accepted Manuscripts* can be found in the **Information for Authors**.

Please note that technical editing may introduce minor changes to the text and/or graphics contained in the manuscript submitted by the author(s) which may alter content, and that the standard **Terms & Conditions** and the **ethical guidelines** that apply to the journal are still applicable. In no event shall the RSC be held responsible for any errors or omissions in these *Accepted Manuscript* manuscripts or any consequences arising from the use of any information contained in them.

ARTICLE TYPE www.rsc.org/xxxxxx | XXXXXXXX

Ioffe-Regel limit and lattice thermal conductivity reduction of high performance $(AgSbTe_2)_{15}(GeTe)_{85}$ thermoelectric materials

Tiejun Zhu,[*a,b,c] Hongli Gao,[a] Yi Chen[a] and Xinbing Zhao,[a,b]

Received (in XXX, XXX) Xth XXXXXXXXX 200X, Accepted Xth XXXXXXXXX 200X
First published on the web Xth XXXXXXXXX 200X
DOI: 10.1039/b000000x

The transport characteristics of high performance $(Ag_xSbTe_{x/2+1.5})_{15}(GeTe)_{85}$ (TAGS-85) (x = 0.4 - 1.2) thermoelectric alloys are investigated. It is found that the carrier mean free path of TAGS-85 materials is comparable to the lattice parameter, indicating that this system has reached the minimum possible mobility, the Ioffe-Regel limit, and the further reduction of grain size will not affect the mobility while benefit to the thermal conductivity reduction. The fine-grained samples are prepared by melt spinning to corroborate the supposition. The carrier mobility and mean free path of melt spun samples are indeed comparable with that in coarse-grained samples, while the lattice thermal conductivity are suppressed effectively as a result of the increasing boundaries and hence phonon scattering. A state-of-the-art ZT of ~ 1.6 is obtained for the melt-spun fine-grained samples and the temperature region of ZT > 1.2 has been broadened notably, which is pretty encouraging for the future applications.

1 Introduction

The need for sources of energy other than fossil fuels has sparked significant research into alternative energy sources and different types of energy conversion technologies in past decades. Thermoelectric (TE) materials have been among the most compelling and challenging materials studied during the last decades. Thermoelectric materials are a class of functional semiconductors which can interconvert heat and electricity. But low efficiency has precluded thermoelectric materials from large scale implementation.[1] The conversion efficiency of TE devices depends on the dimensionless figure of merit $ZT = \alpha^2\sigma T/\kappa$ of the TE materials, where α, σ, κ, T represent the Seebeck coefficient, electrical conductivity, thermal conductivity, and absolute temperature, respectively. Improvement and optimization of the thermoelectric efficiency requires understanding of electrical and thermal transport mechanisms, which has long been elusive.[2]

Various approaches have been used to obtain high ZT values in TE materials. For example, band convergence was applied to increase valley degeneracy, and high performance $PbTe_{1-x}Se_x$ alloys were produced.[3] Multiple-filled $CoSb_3$ exhibited a maximum ZT of 1.7 through the independent optimization of electrical and thermal properties.[4] The recent advances in high performance thermoelectric nanocomposites are achieved mainly through remarkable reduction in the lattice thermal conductivity,[5] such as PbTe,[6] Bi_2Te_3,[7,8] and $CoSb_3$,[9] in which engineered nanoscale features strongly scatter acoustic phonons.

GeTe is a p-type semiconductor in which the electrical conductivity is determined by vacancies on the Ge sites.[10] GeTe is a unique matrix where doping with various elements can significantly affect multiple mechanisms responsible for the thermoelectric transport. Doping of GeTe with Ag and Sb produces a system that is typically written as $(GeTe)_y(AgSbTe_2)_{1-y}$ (TAGS-y). $AgSbTe_2$ is considered to be a solid solution between Ag_2Te and Sb_2Te_3. The composition with the best thermoelectric performance is not the exact stoichiometric TAGS composition but rather corresponds to an optimized Ag/Sb ratio.[11] Ag/Sb ratio serves as a tuning knob to optimize the carrier concentration or microstructure. TAGS has been used in some important applications with the highest figure of merit ZT > 1.4.[1,12] In GeTe based materials, multiply-degenerate Fermi surface pockets provide a route to substantially increase power factor.[13] However, there is little research on the electron and phonon transport characteristics of TAGS alloys.

In this paper, it is found that the carrier mean free path of TAGS-85 materials is comparable to the lattice parameters, indicating that the mobility of this materials system almost reaches the Ioffe-Regel limit. Further grain size reduction will not affect the power factor, while it can suppress effectively the lattice thermal conductivity due to the increased phonon scattering at boundaries. Thus grain refinement by melt spinning is used to reduce the thermal conductivity while maintaining the power factor of TAGS alloys. The maximum ZT value of ~ 1.6 was obtained for the melt spun samples, and the temperature region of ZT > 1.2 has been broadened notably.

2 Experimental details

$(Ag_xSbTe_{x/2+1.5})_{15}(GeTe)_{85}$ (x = 0.4, 0.6, 0.8, 1.0, and 1.2) thermoelectric compounds were synthesized by melting, melt spinning and hot pressing method, where x equals to Ag/Sb ratio. Stoichiometric amounts of Ge, Ag, Sb, and Te single elements with 99.999% purity were weighed and mixed for the desired compositions. The mixture was sealed in an evacuated quartz tube, kept at 1273 K for 10 h and air-cooled to room temperature. The obtained ingots were separated into two parts. One part was directly crushed, pulverized, and hot-pressed in a graphite die at 773 K under 70 MPa pressure for 30 min in vacuum. In the following text, this method will be referred as "AQ", and the samples prepared by this method will be named as "x AQ" samples for different Ag contents. The other part of ingot was treated by melt spinning followed by the same hot-pressing process mentioned above. The melt-spinning process is as

follows: Ingot of suitable weight was put into a quartz tube with a 1.0-mm-diameter nozzle; under the protection of argon atmosphere, the ingots were re-melted and injected onto a copper roller rotating with a linear speed of 40 m/s.[14] The resulting ribbons were pulverized and hot-pressed. This method will be referred as "MS", and the samples prepared by this method will be named as "*x* MS".[14]

Powder X-ray diffraction (XRD) patterns were taken on a Rigaku-D/MAX-2550PC diffractometer with Cu K_α radiation, and the results (Fig. S1) showed that all the samples exhibited clear Bragg peaks of single-phase GeTe with space group R3m (JCPDF no.47-1079). The morphology observation of the melt spun ribbons was taken on a FEI Sirion field emission scanning electron microscope (FESEM). The electrical conductivity and Seebeck coefficient were measured in the temperature range between 300 K and 733 K on a computer-aided apparatus under vacuum using a direct-current (DC) four-probe method and differential voltage/temperature technique, respectively.[15] The thermal conductivity was calculated by using $\kappa = D\rho_D C_P$, where ρ_D is the sample density estimated by an ordinary dimensional and weight measurement procedure. Thermal diffusivity D and specific heat C_P were measured by a laser flash method on a Netzsch LFA457 with a Pyroceram9606 standard.[16] The Hall coefficient R_H measurement was performed at 300 K on a Quantum Design PPMS-9T using a four-probe configuration, with the magnetic field sweeping between ± 4.0 T. Then the carrier concentration p and Hall mobility μ_H were calculated using $p = -(1/eR_H)$ and $\mu_H = \sigma R_H$, respectively.

3. Results and discussion

The temperature dependences of the Seebeck coefficient α, electrical conductivity σ, power factor PF and thermal conductivity κ of the air-cooled and hot pressed TAGS-85 samples are presented in Fig. 1**Error! Reference source not found.**. With the increase of Ag/Sb ratio, the electrical conductivity roughly first increases and then decreases. The electrical conductivity decreases with increasing temperature, indicating a metal-like transport behavior. In the temperature range from 450 K to 550 K, the electrical conductivity underwent a visible "up turn", which is the result of a phase transition from the low-temperature rhombohedra phase to the high-temperature cubic phase.[12] The maximum power factor PF is ~ 34μW/cm.K^2 for $x = 0.6$.

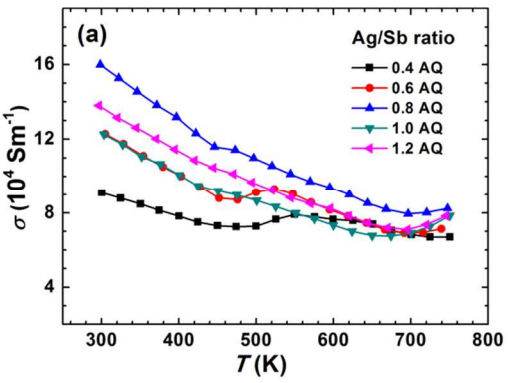

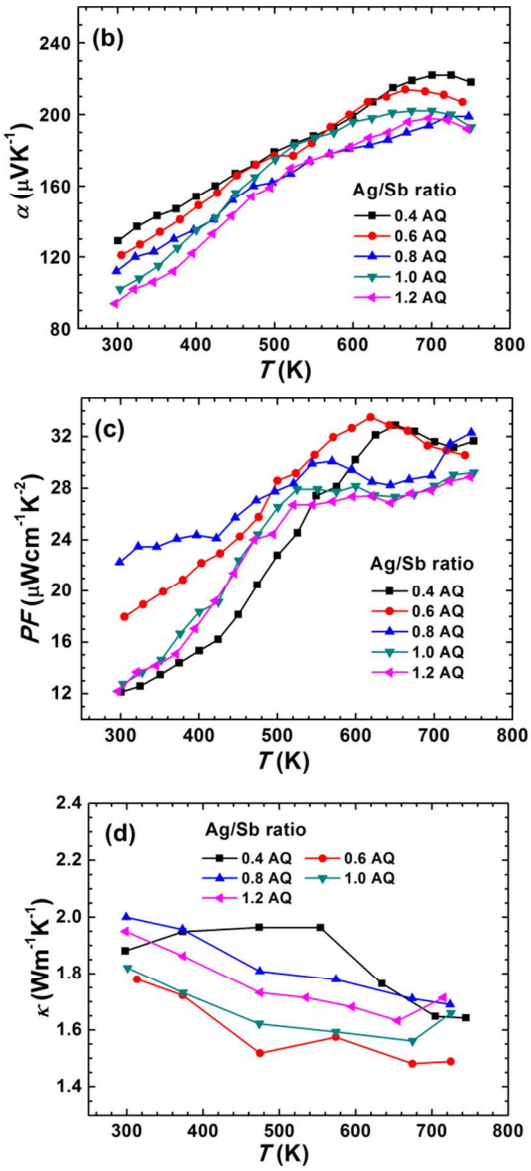

Fig. 1. Temperature dependences of (a) electrical conductivity σ, (b) Seebeck coefficient α, (c) power factor PF, and (d) thermal conductivity κ for slowly cooled TAGS-85 samples.

In order to investigate the carrier transport features of TAGS alloys, the room temperature carrier dependences of Fermi energy E_F, density of states (DOS) effective mass m_d^* and mean free path mfp were calculated. According to previous reports,[17] the scattering factor of TAGS alloys falls into the vicinity of $\lambda = -1/2$, which means that acoustic phonon scattering dominates the carrier transport. The Seebeck coefficient of heavily doped semiconductors is given by the following equation:[1]

$$\alpha = \frac{8\pi^2 k_B^2 T}{3eh^2} m_d^* \left(\frac{\pi}{3p}\right)^{2/3} \quad (1)$$

where k_B is the Boltzmann constant, e the electron charge, h the Planck constant, T the Kelvin temperature, m_d^* the density of states effective mass, and p the hole concentration. If we introduce a characteristic temperature Θ,

$$\Theta = \frac{3h^2}{8\pi^2 k_B m_0}\left(\frac{3p}{\pi}\right)^{2/3} \quad (2)$$

which can be considered as a transformed Fermi temperature $\Theta = 3T_F/\pi^2$, where the Fermi temperature $T_F = E_F/k_B$, Equation (1) can be written as

$$\frac{\alpha}{k_B/e} = \frac{T}{\Theta}\frac{m_d^*}{m_0} \quad (3)$$

The slope of $\alpha/(k_B/e)$ versus T/Θ directly gives the DOS effective mass m_d^*/m_0 as shown in **Error! Reference source not found.**. The carrier concentration of all samples is listed in Table 1. The sample with Ag/Sb ratio of 0.4 has the lowest m_d^*, which is about $3.3m_0$, while samples with higher Ag/Sb ratio hold higher m_d^*.

On the other hand, using the Mott relation[18] for degenerate semiconductors, Seebeck coefficient can be expressed as:

$$\alpha = \frac{\pi^2}{3}\frac{k_B}{e}k_B T\left(\frac{1}{\sigma}\frac{d\sigma}{dE}\right)_{E=E_F} = \frac{\pi^2}{3}\frac{k_B}{e}k_B T\left[\frac{g(E)}{p}+\frac{1}{\mu}\frac{d\mu}{dE}\right]_{E=E_F} \quad (4)$$

where $g(E)$ is the total DOS, μ the carrier mobility. The DOS per pocket is g_p. We have[19]

$$g(E) = \frac{8\pi\left(m_d^*\right)^{3/2}}{h^3}\sqrt{2E} = Ng_p(E) = N\frac{8\pi\left(m_p^*\right)^{3/2}}{h^3}\sqrt{2E} \quad (5)$$

$$p = \frac{\left(m_d^*\right)^{3/2}}{\hbar^3\pi^2}\frac{2\sqrt{2}}{3}E_F^{3/2} \quad (6)$$

where $m_d^* = N^{2/3}m_p^*$ is the total DOS effective mass, including the degeneracy of valleys N and single valley effective mass m_p^*, and the total hole density is $p = Np_p$ (p_p is the density of carriers in each valley). The mobility depends on the mass of each pocket along the direction of the applied electric field. Assuming an isotropic (scalar) mass m_p^* and relaxation time τ, the mobility is expressed as

$$\mu = \frac{e\tau}{m_p^*} = \frac{e\tau_0}{m_p^*}E^{\lambda} \quad (7)$$

By taking Eq. 5-7 into Eq. 4, the expression of Fermi energy is modified to

$$E_F = \left(\lambda+\frac{3}{2}\right)\frac{\pi^2k_B^2T}{3e\alpha} = \frac{\pi^2k_B^2T}{3e\alpha} \quad (8)$$

So the Fermi energy E_F can be calculated from Eq.8 using the experimental Seebeck coefficient α at a certain temperature T, and shown in Fig. 2. The Fermi energy and DOS effective mass increase as Ag/Sb ratio increases, which are consistent with the variation tendency of the carrier concentration. The Fermi level moves deeper into the valance band when the carrier concentration increases.

With the Fermi energy E_F calculated from Eq. 8 and DOS effective mass from Eq. 5, we can further analyze the mean free path *mfp* of charge carriers by the formula

$$mfp = v_F\tau = \sqrt{2E_F m_p^*}\frac{\mu}{e} \quad (9)$$

The mobility μ and carrier mean free path *mfp* for air cooled (AQ) samples are listed in Table 1. At 300 K, the carrier *mfp* is on the same order of magnitude as the lattice constant (~ 6.0 Å) of TAGS-85 materials. By the Ioffe-Regel criterion,[20] this is the lowest limit for metallic conduction, which means that the carrier scattering has reached the highest limit. Further grain refinement will not notably enhance the carrier scattering and reduce the carrier *mfp*, but possibly contribute to the suppression of lattice thermal conductivity.

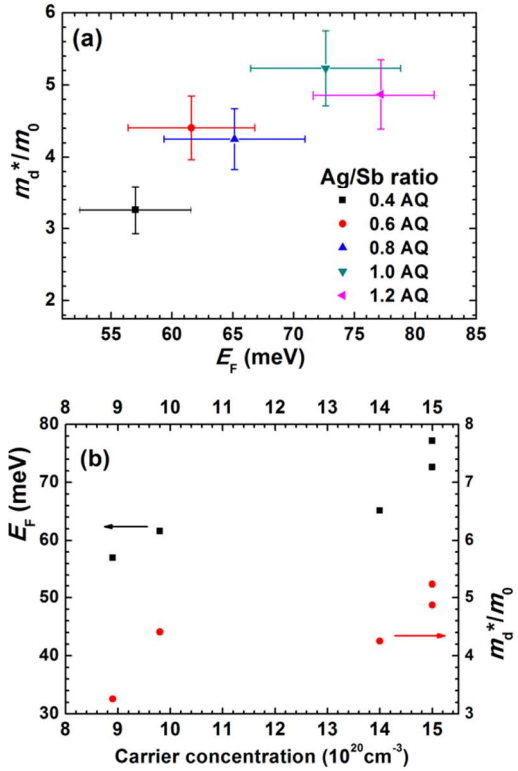

Fig.2 (a) Fermi energy dependence of DOS effective mass; (b) Carrier concentration dependence of Fermi energy E_F and DOS effective mass m_d^* for slowly cooled TAGS-85 samples

Table 1. Carrier density, mobility and mean free path at room temperature for air cooled TAGS-85 samples

Composition	p (10^{20}cm^{-3})	μ (cm^{2}V^{-1}s^{-1})	*mfp* (Å)
0.4 AQ	8.9	6.3	9.3
0.6 AQ	9.8	7.7	12
0.8 AQ	14	7.1	12
1.0 AQ	15	5.0	14
1.2 AQ	15	5.3	11

In order to corroborate the above hypothesis, the fine-grained TAGS-85 samples were prepared by melt spinning. The microstructure observation of the TAGS-85 melt spun ribbons (Fig. S2) shows that the surfaces which contact the copper wheel contain the nanograins of ~ 500 nm and the evenly distributed grains of ~ 2 μm on the other side. Thus, compared with the coarse-grained AQ samples, the MS samples have much smaller grains.

The transport properties of the MS samples are shown in Fig. 3**Error! Reference source not found.**. The Seebeck coefficient of the MS samples is higher than that of the AQ counterparts, while the electrical conductivity is slightly lower, due to the composition fluctuation and hence the carrier density. Thus the power factor of the MS samples is comparable to that of the AQ ones, while the thermal conductivity of the formers is much lower.

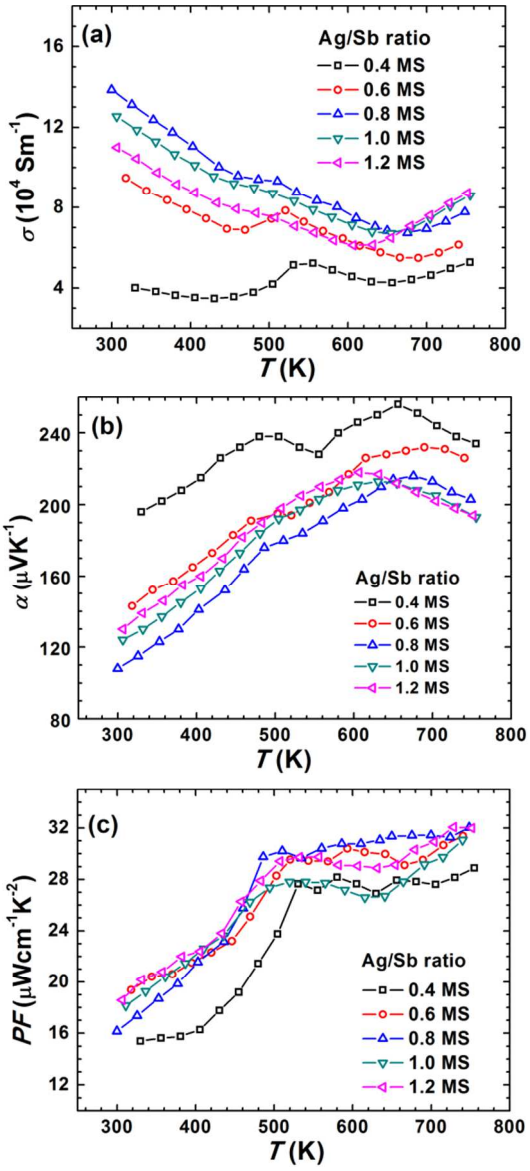

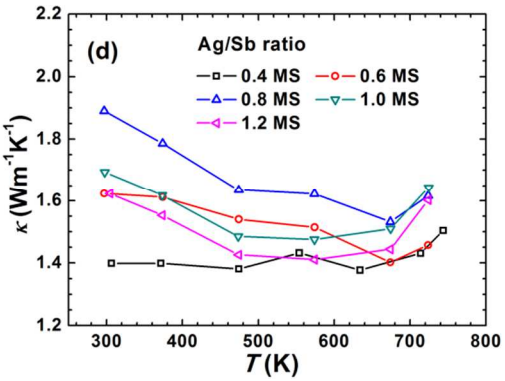

Fig.3 Temperature dependences of (a) electrical conductivity σ, (b) Seebeck coefficient α, (c) power factor PF and (d) thermal conductivity κ for melt spun TAGS-85 samples.

By using Eq. 3 and 8, we calculated the DOS effective mass, Fermi energy and carrier *mfp* of the melt spun TAGS-85 samples, and results are listed in Table 2. Comparing Table 1 and 2, one can find that the carrier *mfp* of these two batches of samples falls on the same level. The melt spun samples have slightly lower mobility than the counterparts because the *mfp* values are close to but still higher than the lattice constants. However, the reduction in grain size does not *significantly* affect the mobility, which is consistent with the above conjecture that the carrier transport in TAGS-85 alloys has *almost* reached the Ioffe-Regel limit.

Table 2 Room temperature carrier density p, mobility μ and mean free path *mfp* for melt spun TAGS samples.

Composition	p (10^{20}cm^{-3})	E_F (meV)	m_d^*/m_0	μ (cm^{2}V^{-1}s^{-1})	*mfp* (Å)
0.4 MS	4.0	41.13	2.03	6.4	6.2
0.6 MS	8.6	54.39	3.87	7.0	11
0.8 MS	13	67.87	5.09	6.7	13
1.0 MS	12	60.39	5.01	6.5	12
1.2 MS	13	57.64	5.44	5.5	10

The total thermal conductivity κ is the sum of a lattice component κ_L and a carrier component κ_c, $\kappa = \kappa_c + \kappa_L$. The carrier term κ_c is related to the electrical conductivity via the Wiedemann-Franz law $\kappa_c = L\sigma T$, where L is the Lorenz number. The Lorenz number on the basis of Fermi-Dirac statistics can be expressed as follows:[21]

$$L = \left(\frac{k_B}{e}\right)^2 \left[\left(\lambda+\frac{7}{2}\right)F_{\lambda+5/2}(\zeta^*)/\left(\lambda+\frac{3}{2}\right)F_{\lambda+1/2}(\zeta^*) - \delta^2(\zeta^*)\right] \quad (10)$$

$$\delta(\zeta^*) = \frac{\left(\lambda+\frac{5}{2}\right)F_{\lambda+3/2}(\zeta^*)}{\left(\lambda+\frac{3}{2}\right)F_{\lambda+1/2}(\zeta^*)} \quad (11)$$

where λ is the scattering factor (here $\lambda = -1/2$),and $\zeta^* = E_F/(k_BT)$ is the reduce Fermi energy. E_F can be calculated from Eq. 8. The

calculated reduced Fermi energy ζ^* and Lorenz number L are summarized in Table 3.

From Table 3, it can be seen that the Lorenz number hovers ~ 2.0×10^{-8} V^2K^{-2} in the wide carrier concentration range of all samples. We fix the Lorenz number as 2.0×10^{-8} V^2K^{-2} in our subsequent lattice thermal conductivity calculation.

Table 3 Room temperature Lorenz number and reduced Fermi energy for TAGS-85 materials with different carrier concentrations.

composition	p (10^{20} cm^{-3})	ζ^*	L (10^{-8} V^2K^{-2})
0.4 MS	4.0	1.59	1.82
0.6 MS	8.6	2.10	1.87
0.8 MS	13	2.62	1.94
1.0 MS	12	2.33	1.91
1.2 MS	13	2.23	1.84

Error! Reference source not found. Fig. 4 shows the lattice thermal conductivity of the air cooled and melt spun TAGS-85 samples at room temperature. Compared to AQ samples, the lattice thermal conductivity of MS samples is evidently lower over a wide Ag/Sb ratio. For samples $x = 0.8$, the lattice thermal conductivity is very close, possibly due to the compositional fluctuation. This result approves our hypothesis that for TAGS-85 materials the scattering of carriers almost reaches the Ioffe-Regel limit as the mean free path almost approaches the interatomic distance, and the grain refinement will not significantly affect the electrical transport properties, but it can reduce the lattice thermal conductivity.

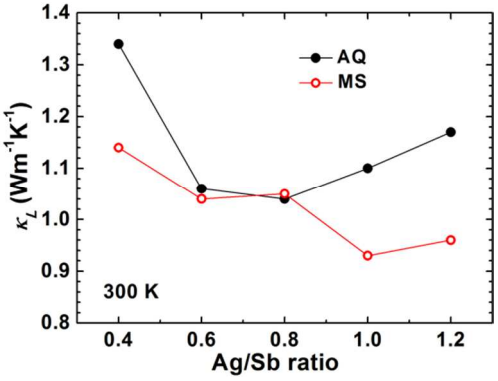

Fig. 4. Lattice thermal conductivity at room temperature for air cooled and melt spun TAGS-85 samples with different Ag/Sb ratios.

The dimensionless figure of merit ZT of all samples is shown in Fig.5**Error! Reference source not found.**. Owing to the preservation of good power factor and reduction of thermal conductivity, the ZT values of the melt spun samples was improved, and a maximum ZT of ~1.6 was obtained at ~ 750 K. At the same time the temperature region of $ZT > 1.2$ has been broadened notably, which is pretty encouraging for the future applications.

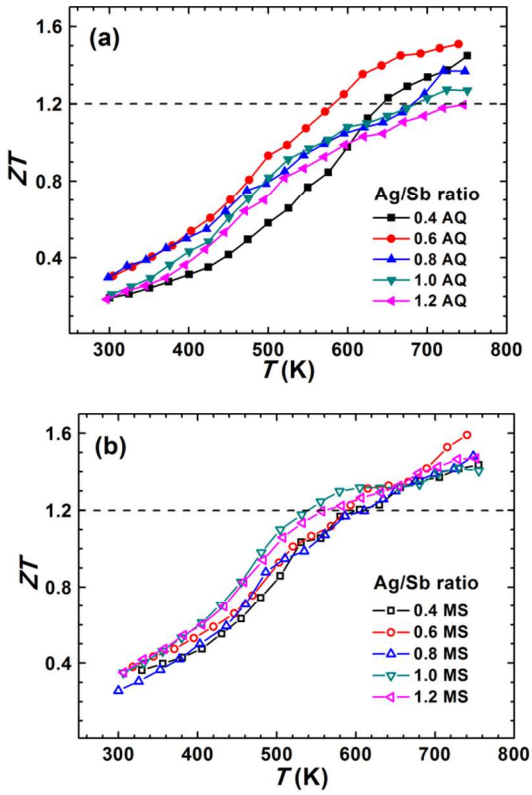

Fig. 5. Temperature dependence of ZT for (a) air cooled and (b) melt spun TAGS-85 samples.

4 Conclusions

In summary, $(Ag_xSbTe_{x/2+1.5})_{15}(GeTe)_{85}$ (x = 0.4 - 1.2) thermoelectric materials have been fabricated by air cooling or melt spinning method, combined with a subsequent hot-pressing. The electrical and thermal transport properties were investigated systematically in the temperature range of 300 ~ 750 K. We found that the carrier mean free path of TAGS-85 materials is comparable to the lattice parameter, implying that the materials have reached the minimum possible mobility, the Ioffe-Regel limit. The carrier mobility and mean free path of fine-grained samples by melt spinning are comparable with those in coarse-grained samples by slow cooling, while the lattice thermal conductivity of the former is suppressed effectively as a result of grain refinement to enhance the phonon scattering at boundaries. The ZT values of the melt spun samples were improved and reached ~ 1.6 at 750 K. The temperature span of $ZT > 1.2$ has been enlarged notably, which is pretty encouraging for the future applications.

Acknowledgements

This work is supported by the National Basic Research Program of China (2013CB632503), the Nature Science Foundation of China (Grant Nos 51171171 and 51271165), the Program for Innovative Research Team in University of Ministry of Education of China, the Research Fund for the Doctoral Program of Higher Education of China (No. 20120101110082), and the Program for New Century Excellent Talents in University (NCET-12-0495).

Notes and references

[a]*State Key Laboratory of Silicon Materials, Department of Materials Science and Engineering, Zhejiang University, Hangzhou 310027, China*
[b]*Key Laboratory of Advanced Materials and Applications for Batteries of Zhejiang Province, Zhejiang University, Hangzhou 310027, China*
[c]*Cyrus Tang Center for Sensor Materials and Applications, Zhejiang University, Hangzhou 310027, China*

Corresponding author: zhutj@zju.edu.cn

1 G. J. Snyder and E. S. Toberer, *Nat. Mater.,* 2008, **7**, 105-114.
2 D. J. Singh and I. Terasaki, *Nat. Mater.,* 2008, **7**, 616-617.
3 Yu I. Ravich, B.A. Efimova and I.A. Smirnov, *Semiconducting Lead Chalcogenides*, Plenum Press, New York, 1970.
4 X. Shi, J. Yang, J. R. Salvador, M. F. Chi, J. Y. Cho, H. Wang, S. Q. Bai, J. H. Yang, W. Q. Zhang and L. D. Chen, *J. Am. Chem. Soc.*, 2011, **133**, 7837-7846.
5 M. G. Kanatzidis, K. F. Hsu, S. Loo, F. Guo, W. Chen, J. S. Dyck, C. Uher, T. Hogan and E. K. Polychroniadis, *Science*, 2004, **303**, 818-821.
6 K. Ahn, M. K. Han, J. Q. He, J. Androulakis, S. Ballikaya, C. Uher, V. P. Dravid and M. G. Kanatzidis, *J. Am. Chem. Soc.*, 2010, **132**, 5227-5235.
7 X.B. Zhao, X.H. Ji, Y.H. Zhang, T.J. Zhu**,** J.P. Tu and X.B. Zhang, *Appl. Phys. Lett.*, 2005, **86**, 062111.
8 B. Poudel, Q. Hao, Y. Ma, Y. C. Lan, A. Minnich, B. Yu, X. Yan, D. Z. Wang, A. Muto, D. Vashaee, X. Y. Chen, J. M. Liu, M. S. Dresselhaus, G. Chen and Z. F. Ren, *Science*, 2008, **320**, 634-638.
9 X. Y. Zhou, G. Y. Wang, L. Zhang, H. Chi, X. L. Su, J. Sakamoto and C. Uher, *J. Mater. Chem.*, 2012, **22**, 2958-2964.
10 E. M. Levin, B. A. Cook, J. L. Harringa, S. L. Bud'ko, R. Venkatasubramanian and K. Schmidt-Rohr, *Adv. Funct. Mater.*, 2011, **21**, 441-447.
11 G. C. Christakudis, S. K. Plachkova, L. E. Shelimova and E. S. Avilov, *Phys. Status. Solidi. A*, 1991, **128**, 465-471.
12 B. A. Cook, M. J. Kramer, X. Wei, J. L. Harringa and E. M. Levin, *J. Appl. Phys.*, 2007, **101**, 053715.
13 R. Tsu, W. E. Howard and L. Esaki, *Phys. Rev.*, 1968, **172**, 779-788.
14 Y. Chen, T. J. Zhu, S. H. Yang, S. N. Zhang, W. Miao and X. B. Zhao, *J. Electron. Mater.*, 2010, **39**, 1719-1723.
15 S. H. Yang, T. J. Zhu, T. Sun, S. N. Zhang, X. B. Zhao and J. He, *Nanotechnology*, 2008, **19,** 245707.
16 C. B. Vining, A. Zoltan and J. W. Vandersande, *Int. J. Thermophys.*, 1989, **10**, 259-268.
17 S. K. Plachkova and T. I. Georgiev, *Phys. Status. Solidi. A*, 1993, **136**, 509-528.
18 T. M. Tritt, *Annu. Rev. Mater. Res.*, 2011, **41**, 14.1-14.26.
19 V. I. Fistul, *Heavily Doped Semiconductors*, Plenum Press, New York, 1969.
20 M. Gurvitch, *Phys. Rev. B*, 1981, **24**, 7404-7407.
21 P. Pichanusakorn and P. Bandaru, *Mater. Sci. Eng. R.*, 2010, **67**,19-63.